

A Nonquadratic Regularization-based Technique for Joint SAR Imaging and Model Error Correction

N. Özben Önhon and Müjdat Çetin

Faculty of Engineering and Natural Sciences, Sabancı University, Orhanlı, Tuzla, 34956
Istanbul, Turkey

ABSTRACT

Regularization based image reconstruction algorithms have successfully been applied to the synthetic aperture radar (SAR) imaging problem. Such algorithms assume that the mathematical model of the imaging system is perfectly known. However, in practice, it is very common to encounter various types of model errors. One predominant example is phase errors which appear either due to inexact measurement of the location of the SAR sensing platform, or due to effects of propagation through atmospheric turbulence. We propose a nonquadratic regularization-based framework for joint image formation and model error correction. This framework leads to an iterative algorithm, which cycles through steps of image formation and model parameter estimation. This approach offers advantages over autofocus techniques that involve post-processing of a conventionally formed image. We present results on synthetic scenes, as well as the Air Force Research Laboratory (AFRL) Backhoe data set, demonstrating the effectiveness of the proposed approach.

Keywords: SAR imaging, phase errors, regularization based image reconstruction

1. INTRODUCTION

A significant part of the remote sensing applications involve the Synthetic Aperture Radar (SAR) imaging. In SAR imaging, model uncertainties cause undesired artifacts in the formed imagery. For SAR imaging one of the most important model uncertainties is due to demodulation time errors. Demodulation time is the time required for the signal transmitted by the SAR sensor to propagate from the SAR platform to the field and back. The reasons for demodulation time errors are the uncertainties in the measurement of the distance between the SAR platform and the field or random delays in the signal due to propagation in atmospheric turbulence. Demodulation time errors appear in the frequency domain SAR data as phase errors. In the reconstructed images the effect of phase errors is seen in the cross range direction. While low frequency phase errors result in a blurring of the SAR image, high frequency phase errors cause a loss of contrast in the reconstructed image [1]. There are many algorithms which are called autofocus techniques developed to remove the phase error effects in SAR images [2-7]. Mostly they are based on post-processing of the image, reconstructed by conventional imaging, e.g. polar format algorithm. One of the most well known techniques known as Phase gradient autofocus (PGA) estimates phase errors using the data obtained by isolating many single defocused targets via center-shifting and windowing operations [2]. There are also many autofocus techniques which optimize different sharpness metrics of the defocused image intensity [3-5]. These techniques have been shown to give good results. However, in the case of incomplete data or sparse aperture, conventional imaging does not perform well. Therefore, in such cases, when the SAR data include phase errors it may not be so effective to estimate phase errors from the image produced by conventional imaging. On the other hand regularization based image reconstruction techniques have successfully been applied to SAR imaging [8]. They effectively deal with the noisy SAR data even in cases where the data are incomplete. Additionally, they produce feature enhanced images by using prior information regarding the nature of the features of interest. Compared to conventional imaging they produce images with increased

Further author information:

N. Özben Önhon: E-mail: onhon@su.sabanciuniv.edu

Müjdat Çetin : E-mail: mçetin@sabanciuniv.edu

resolution, reduced sidelobes and reduced speckle. Motivated by such advantages of regularization based image reconstruction techniques, we propose a nonquadratic regularization based framework for joint image formation and phase error correction. A cost function depending on both image and phase error is minimized by an iterative algorithm. In the first step of every iteration an estimate of the field is found. Given the field estimate, in the second step the phase error for that iteration is estimated and used to update the model matrix. We present results on a synthetic scene, as well as the Slicy data [9], and the Air Force Research Laboratory (AFRL) Backhoe data set [10]. The results show that the proposed method can deal with structured as well as random phase errors.

2. SAR IMAGE MODEL

SAR is an imaging radar. It is generally mounted on an airplane or satellite. On its flight path the SAR sensor transmits regularly a signal to the field and then receives the reflected signals from the field. Let us focus on spotlight-mode SAR and consider a chirp signal transmitted at every aperture position

$$s(t) = Re \{ \exp[j(\omega_0 t + \alpha t^2)] \} \quad (1)$$

where ω_0 is the center frequency and 2α is the so called chirp-rate. The received signal $q_\theta(t)$ is the convolution of the transmitted chirp signal with the projection $p_\theta(u)$ of the field at that observation angle.

$$q_\theta(t) = Re \left\{ \int p_\theta(u) \exp[j[\omega_0(t - \tau_0 - \tau(u)) + \alpha(t - \tau_0 - \tau(u))^2]] du \right\} \quad (2)$$

If we let the distance from the SAR platform to the center of the field be R and the distance from the SAR platform to a scatterer along the range be $R+u$ then the delay for the returned signal can be defined as $\tau_0 + \tau(u)$ where $\tau_0 = \frac{2R}{c}$ and $\tau(u) = \frac{2u}{c}$. The SAR data used for imaging is obtained after some pre-processing of the returned signal. To perform it, first, the returned signal is multiplied with the quadrature and in-phase components of the signal returned from the patch center, that are shown in (3), and then the result is filtered with a low-pass filter.

$$\begin{aligned} c_I(t) &= \cos(\omega(t - \tau_0) + \alpha(t - \tau_0)^2) \\ c_Q(t) &= -\sin(\omega(t - \tau_0) + \alpha(t - \tau_0)^2) \end{aligned} \quad (3)$$

If the spatial frequency variable U is defined as

$$U = \frac{2}{c}(\omega_0 + 2\alpha(t - \tau_0)) \quad (4)$$

the signal $r_\theta(t)$, obtained after the low-pass filtering, can be written as in (5), [1].

$$Z(U) = r_\theta(t) = \int p_\theta(u) e^{-juU} du \quad (5)$$

$r_\theta(t)$ is the one dimensional Fourier transform of the projection $p_\theta(u)$ for that observation angle. Based on the projection-slice theorem [11] known from the CT (Computerized Tomography), $r_\theta(t)$ is a band-limited slice taken from the 2D frequency data at the observation angle θ . Based on this observation, we can write the relation between the field and the SAR data as follows:

$$r_\theta(t) = \iint_{x^2+y^2 \leq L^2} f(x, y) \exp\{-jU(x \cos \theta + y \sin \theta)\} dx dy \quad (6)$$

Here, we observe that all of the returned signals constitute a patch from the two dimensional Fourier transform of the corresponding field. This expression can be written in a compact form as $r_\theta(t) = (C_\theta f(x, y))(t)$.

The corresponding discrete model is as follows [8].

$$\begin{bmatrix} r_{\theta 1} \\ r_{\theta 2} \\ \vdots \\ r_{\theta M} \end{bmatrix} = \begin{bmatrix} C_{\theta 1} \\ C_{\theta 2} \\ \vdots \\ C_{\theta M} \end{bmatrix} f \quad (7)$$

where $r_{\theta m}$ is the vector of observed samples, $C_{\theta m}$ is discretized approximation to the continuous observation kernel $C_{\theta m}$ and f is a vector representing the unknown sampled reflectivity image. If we consider that there is also measurement noise, the observation model becomes

$$g = Cf + v \quad (8)$$

where v stands for measurement noise which is assumed to be white Gaussian noise and g is the noisy observation. After expressing the SAR imaging system in this form, regularization based image reconstruction can be used for imaging.

3. PHASE ERRORS

All of the expressions so far were based on the assumption that there is no uncertainty or error in the imaging model, i.e. it was assumed that the model matrix C is known exactly. However, in many situations, this assumption is not valid and there are some errors in the model. One particular type of error we consider here is phase errors. Phase errors appear when the so called demodulation time which is the time required for the transmitted signal to travel from the SAR platform to the field and back cannot be determined exactly. In this case, during preprocessing, the received signals are multiplied with

$$\begin{aligned} & \cos(\omega(t - \tau_0 + \epsilon) + \alpha(t - \tau_0 + \epsilon)^2) \\ & -\sin(\omega(t - \tau_0 + \epsilon) + \alpha(t - \tau_0 + \epsilon)^2) \end{aligned} \quad (9)$$

instead of the expressions in (3). Here, ϵ is the demodulation time error. It occurs when the distance between the SAR platform and the field cannot be measured exactly or in the case of random delays in the signal due to propagation in atmospheric turbulence. The demodulation time error results in phase errors in the SAR data obtained after preprocessing of the received signal. After some approximations, the relationship between the erroneous and error-free phase histories is obtained as in (10) [1].

$$Z_\epsilon(U) = e^{j\frac{\epsilon\omega}{2}U} Z(U) \quad (10)$$

If we substitute the expression in (4) into (10) we find

$$Z_\epsilon(U) = e^{j\epsilon\omega_0} e^{j\epsilon(2\alpha(t-\tau_0))} Z(U) \quad (11)$$

The value of $(2\alpha(t - \tau_0))$ is generally very small as compared to ω_0 , so if it is neglected, we obtain

$$Z_\epsilon(U) = e^{j\phi} Z(U) \quad (12)$$

where $\phi = \epsilon\omega_0$ is the phase error and it is different for every aperture position which means that it affects the reconstructed image along the cross-range. Depending on the structure of the phase error across the synthetic aperture it can cause blurring or loss of contrast in the image.

4. REGULARIZATION BASED IMAGE RECONSTRUCTION

Regularization based image reconstruction techniques produce feature enhanced images. It is achieved by incorporating a prior information of the field to the image formation problem. There are many specific cases of regularization based image reconstruction. Here we consider one of them which provides reconstructions with good energy concentration. It is performed by solving the following optimization problem

$$\hat{f} = \arg \min_f \|g - Cf\|_2^2 + \lambda \|f\|_k^k \quad (13)$$

where λ is the regularization parameter. This type of regularization is usually preferred when the scene is sparse since it produces point-enhanced images. For $k=2$ the expression in (13) is Tikhonov regularization and the estimate of f can be found in closed form. If $k < 2$ the problem is solved iteratively. However, for point-enhanced imaging it has been shown that $l_k - norm$ constraints where $k < 2$ result in higher resolution spectral estimates compared to $l_2 - norm$ case. Moreover, smaller value of k implies less penalty on large pixel values as compared to larger k [8].

5. PROPOSED METHOD

The effectiveness of regularization based image reconstruction techniques for SAR image formation has been shown. Compared to conventional imaging (polar format algorithm) they offer a number of advantages. In conventional imaging the image is formed by interpolating the SAR data from the polar grid to a rectangular grid and then taking its 2D inverse Fourier transform. Images formed by conventional imaging usually suffer from speckle and sidelobe artifacts. Furthermore the resolution of the images is limited by the SAR system bandwidth. However we know that regularization based image formation techniques can deal with these problems. Therefore we propose a method which removes phase errors, while using regularization based image reconstruction for image formation. This approach offers advantages also in scenarios such as sparse aperture imaging. Due to the reasons explained in the previous section we used $l_1 - norm$ regularization. The proposed algorithm is an iterative algorithm, which cycles through steps of image formation and phase error estimation and compensation. It is based on the minimization of the following cost function, with respect to ϕ and f using coordinate descent technique.

$$J(f, \phi) = \|g - C(\phi)f\|_2^2 + \lambda \|f\|_1 \quad (14)$$

In the first step of every iteration the cost function $J(f, \phi)$ is minimized with respect to f .

$$\hat{f}^{(n+1)} = \arg \min_f J(f, \phi^{(n)}) \Rightarrow \arg \min_f \left\| g - C(\phi^{(n)})f \right\|_2^2 + \lambda \|f\|_1 \quad (15)$$

where n denotes the iteration number. To avoid problems due to nondifferentiability of the $l_1 - norm$ at the origin, a smooth approximation shown in (16) is used [8].

$$\|f\|_1 \approx \sum_{i=1}^K (|f_i|^2 + \beta)^{1/2} \quad (16)$$

where β is a nonnegative small constant. In each iteration, the field estimate is obtained as

$$\hat{f}^{(n+1)} = \left(C(\hat{\phi}^{(n)})^H C(\hat{\phi}^{(n)}) + \lambda W(\hat{f}^{(n)}) \right)^{-1} C(\hat{\phi}^{(n)})^H g \quad (17)$$

where $W(\hat{f}^{(n)})$ is a diagonal matrix as given in (18)

$$W(\hat{f}^{(n)}) = \text{diag} \left[\frac{1}{(|\hat{f}_i^{(n)}|^2 + \beta)^{1/2}} \dots \dots \dots \frac{1}{(|\hat{f}_K^{(n)}|^2 + \beta)^{1/2}} \right] \quad (18)$$

Note that $C(\phi^{(n)})$ denotes the model matrix corresponding to the phase error obtained in the n -th iteration. For the first iteration $\phi^{(0)} = 0$. Given the field estimate, in the second step, the phase error for the current iteration is estimated for every aperture position by solving the following optimization problem

$$\widehat{\Delta\phi}_m^{(n+1)} = \arg \min_{\Delta\phi_m} J(\hat{f}^{(n+1)}, \Delta\phi_m) \Rightarrow \widehat{\Delta\phi}_m^{(n+1)} = \arg \min_{\Delta\phi_m} \left\| g_m - \exp(j\Delta\phi_m) C_m(\hat{\phi}_m^{(n)}) \hat{f}^{(n+1)} \right\|_2^2 \quad (19)$$

for $m = 1, 2, \dots, M$

where $\widehat{\Delta\phi}_m^{(n+1)}$ denotes the incremental phase error estimate for the m -th aperture position in the iteration $(n+1)$. In (19), g_m and $C(\phi_m)$ stand for the part belonging to the m -th aperture position of the SAR data and the model matrix, respectively. The overall phase error estimate for the m -th aperture position is the addition of the incremental phase error estimates found in each iteration for the m -th aperture position. The optimization problem in (19) can be solved in closed form for every aperture position. After evaluating the norm expression in (19) and rearranging it, we end up with the following.

$$\widehat{\Delta\phi}_m^{(n+1)} = \arg \min_{\Delta\phi_m} (g_m^H g_m - 2\sqrt{R^2 + I^2} \cos[\Delta\phi_m + \arctan(\frac{-I}{R})] + \hat{f}^H C_m(\hat{\phi}_m^{(n)})^H C_m(\hat{\phi}_m^{(n)}) \hat{f}) \quad (20)$$

where

$$R = \text{Re}\{\hat{f}^H C_m(\hat{\phi}_m^{(n)})^H g_m\} \quad I = \text{Im}\{\hat{f}^H C_m(\hat{\phi}_m^{(n)})^H g_m\} \quad (21)$$

We know that negative cosine has its minimum at zero and integer multiples of 2π , so if we set argument of the cosine to zero, we find the phase error estimate as given in (22) for the corresponding aperture position.

$$\widehat{\Delta\phi}_m^{(n+1)} = -\arctan(\frac{-I}{R}) \quad (22)$$

Using the incremental phase error estimate, the overall phase error and the model matrix are updated as follows:

$$\hat{\phi}_m^{(n+1)} = \widehat{\Delta\phi}_m^{(n+1)} + \hat{\phi}_m^{(n)} \quad (23)$$

$$C_m(\hat{\phi}_m^{(n+1)}) = \exp(j\widehat{\Delta\phi}_m^{(n+1)}) C_m(\hat{\phi}_m^{(n)}) \quad (24)$$

We increase n and turn back to the optimization problem in (15) for the field estimate in the next iteration. All of these steps are repeated until the ratio

$$\left\| \hat{f}^{(n+1)} - \hat{f}^{(n)} \right\|_2^2 / \left\| \hat{f}^{(n)} \right\|_2^2 \quad (25)$$

is less than a pre-determined threshold.

6. EXPERIMENTAL RESULTS

The proposed method is applied to a synthetic scene and also to the Backhoe dataset. For the synthetic example, we generate a 32x32 sparse scene shown in Figure 1(a). To generate synthetic SAR data we construct a SAR system model with the parameters given in Table 1. Based on this SAR observation model, SAR returns from the synthetic scene are produced and white Gaussian noise is added so that SNR is 30dB. We have performed experiments for four different types of phase errors. For the case of no phase errors, the reconstruction with conventional imaging is shown in Figure 1(b). Results by conventional imaging and by the proposed method for different types of phase errors are shown in Figure 2. Conventionally reconstructed images suffer from degradation due to phase errors. The results show the effectiveness of the proposed

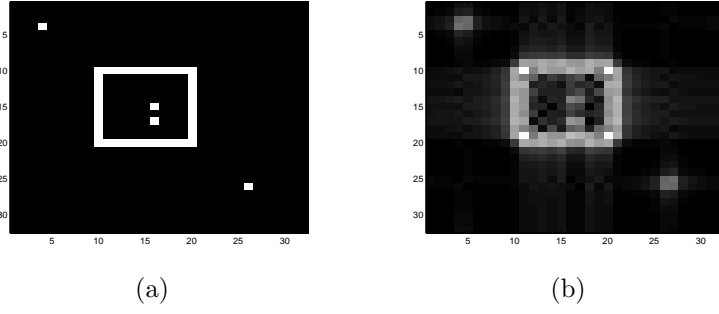


Figure 1. (a) The original scene (b) Conventionally reconstructed image when there is no phase error.

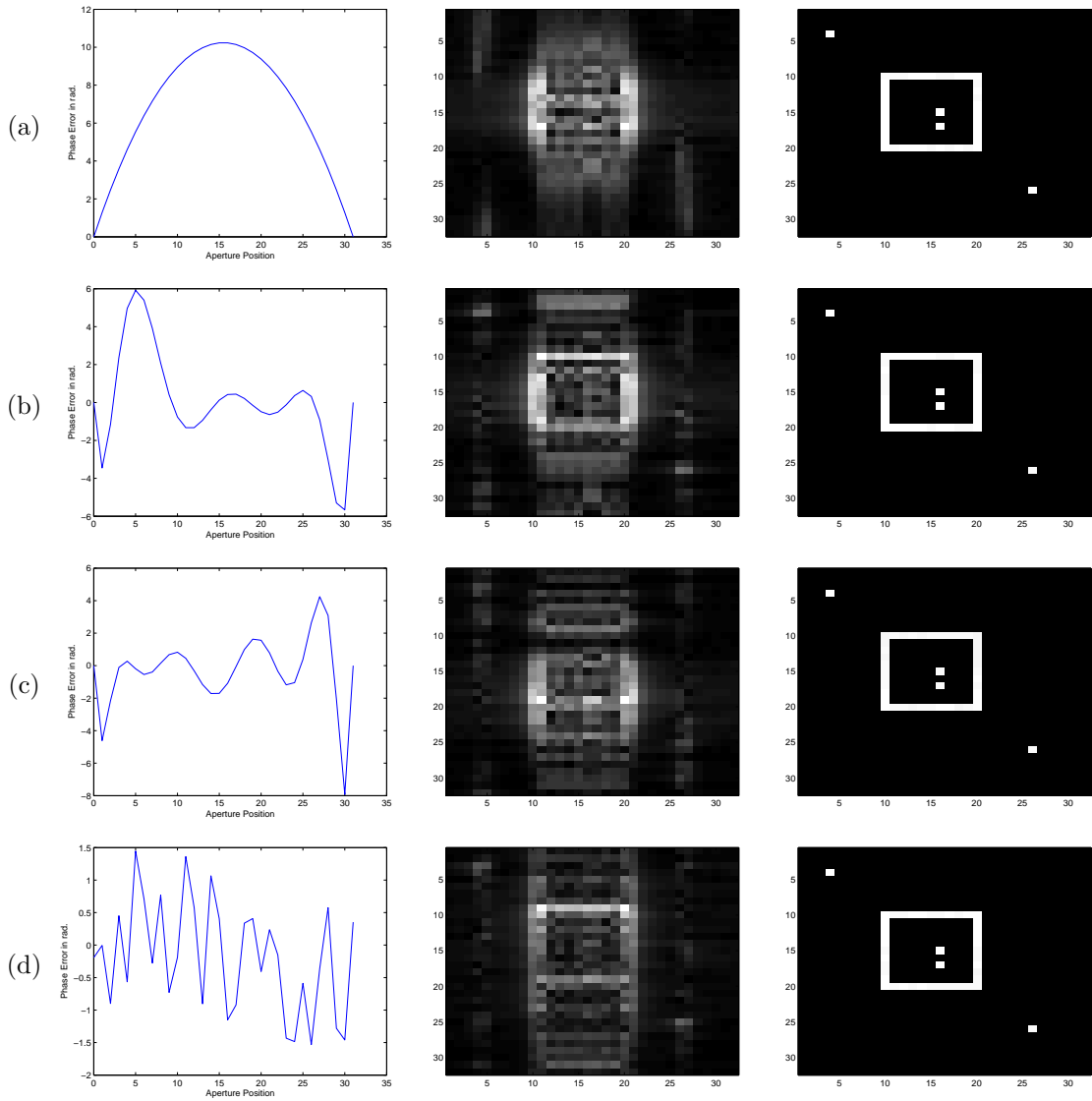


Figure 2. Left- Phase error, Middle- Images reconstructed with conventional imaging, Left- Images reconstructed with the proposed method. (a) Results for quadratic phase error (b) Results for an 8th order polynomial phase error (c) Results for a 10th order polynomial phase error (d) Results for a phase error uniformly distributed in $[-\pi/2, \pi/2]$.

Table 1. SAR System Parameters

carrier frequency (ω_0)	$2\pi \times 10^{10} \text{ rad/s}$
chirp rate (2α)	$2\pi \times 10^{12} \text{ rad/s}^2$
pulse duration (T_p)	$4 \times 10^{-4} \text{ sec.}$
angular range ($\Delta\theta$)	2.3°

method. As seen in Figure 2, it is not possible to visually distinguish the images formed by the proposed method from the original scene.

In addition to the synthetic scene, we present some results on the Slicy data. Figure 3 shows the images formed by conventional imaging and point-enhanced imaging when there is no phase error. The images are reconstructed using data from an angular range of 10 degrees and a bandwidth of 1GHz. In Figure 4, the results for four different phase errors are presented for the case when there are phase errors. The results show that the phase error removal is performed effectively.

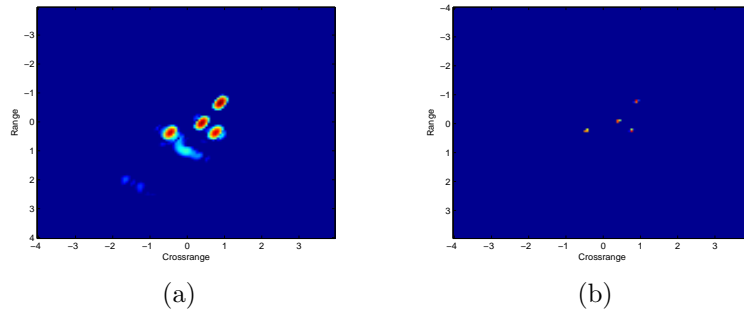


Figure 3. (a) Conventional imaging of Slicy data without any phase errors (b) Point-enhanced imaging of Slicy data without any phase errors.

Another dataset on which we present results is the Backhoe dataset. To deal with the wide-angle observation in the Backhoe dataset, we incorporate the subaperture-based composite imaging approach of [12] into our framework. For a random phase error uniformly distributed in $[-\pi/2, \pi/2]$, the results for the bandwidths 2 GHz., 1 GHz. and 500 MHz. are shown in Figure 5. In Figure 5(a) and 5(b) the conventional imaging and point enhanced imaging results are presented respectively, for the case of no phase error. Here it is seen that point enhanced imaging produce images with higher resolution compared to conventional imaging. Figure 5(c) shows the images corrupted with phase error and Figure 5(d) shows the images reconstructed by the proposed method. As seen in the results, for all of three bandwidths, phase errors are estimated and corrected successfully.

7. CONCLUSION

We proposed a nonquadratic regularization based technique for joint SAR image formation and phase error correction. It is an iterative algorithm, which cycles through steps of image formation and model parameter estimation. Considering the sparsity of the scene, l_1 - norm regularization is used for a point-enhanced high resolution imaging. The method corrects the phase errors during the image formation process while it provides images with enhanced features. The presented results on a synthetic scene, as well as the Slicy data and the Backhoe data set, show the effectiveness of the proposed approach. In future work, we want to extend our current method in a number of ways. Our current formulation does not include any prior information about the phase errors and may suffer from some ambiguity in phase. To deal with that, the

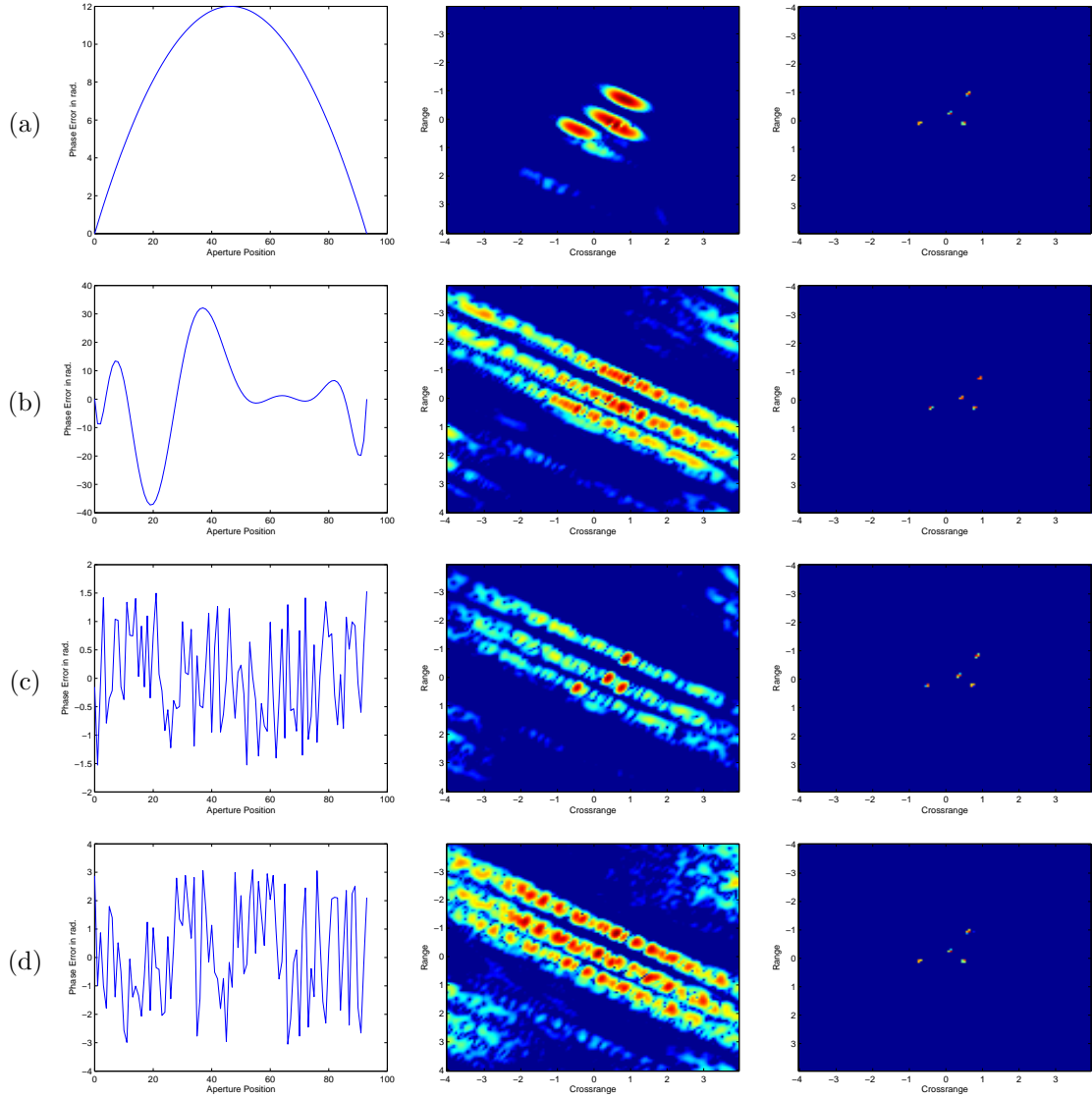


Figure 4. Left- Phase error, Middle- Images reconstructed with conventional imaging, Right- Images reconstructed using the proposed method. (a) Results for quadratic phase error (b) Results for a 10th order polynomial phase error (c) Results for a phase error uniformly distributed in $[-\pi/2, \pi/2]$ (d) Results for a phase error uniformly distributed in $[-\pi, \pi]$.

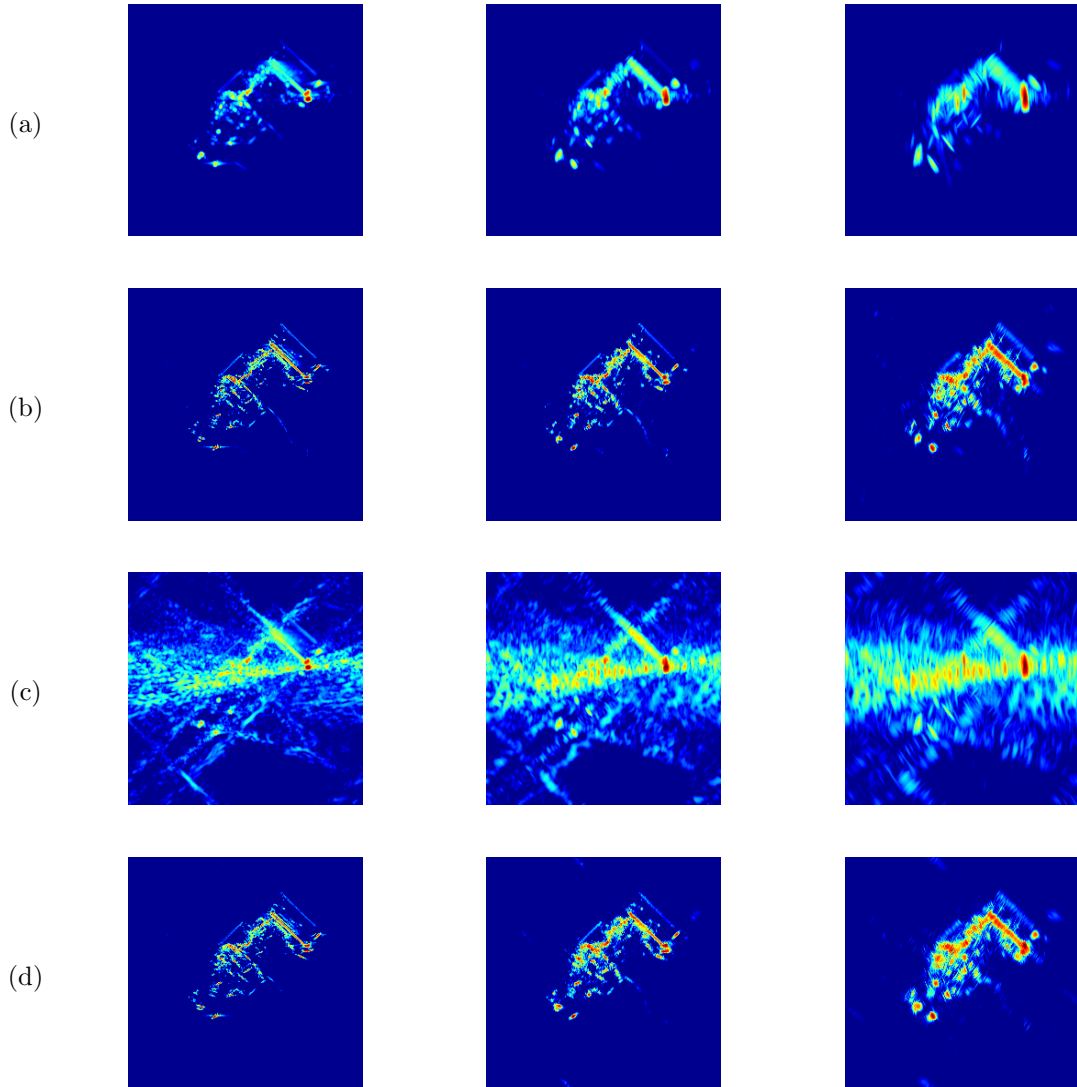


Figure 5. Results for data with various bandwidths: Left-2 GHz., Middle-1 GHz., Right-500 MHz., a) Conventional composite images when there is no phase error b) Point-enhanced composite images when there is no phase error c) Conventional composite images when there is phase error d) Images reconstructed by the proposed method when there is phase error.

method can be extended by incorporating a prior knowledge of the phase error into the optimization problem. Moreover, the current framework can be modified for other type of model errors in SAR.

ACKNOWLEDGMENTS

This work was partially supported by the Scientific and Technological Research Council of Turkey under Grant 105E090, and by a Turkish Academy of Sciences Distinguished Young Scientist Award.

REFERENCES

1. C. V. Jakowatz, Jr., D. E. Wahl, P. H. Eichel, D. C. Ghiglia, and P. A Thompson, *Spotlight-Mode Synthetic Aperture Radar: A Signal Processing Approach*. Norwell, MA: Kluwer, 1996.
2. D.E. Wahl, P. H. Eichel, D. C. Ghiglia and C. V. Jakowatz, "Phase Gradient Autofocus - A robust tool for high resolution SAR phase correction," *IEEE Trans. Aerosp. Electron.Syst.*, vol.30, no. 3, Jul. 1994.
3. L. Xi, L. Guosui, and J. Ni, "Autofocusing of ISAR images based on entropy minimization," *IEEE Trans. Aerosp. Electron. Syst.*, vol. 35, no. 10, pp. 1240-1252,Oct. 1999.
4. F. Berizzi and G. Corsini, "Autofocusing of inverse synthetic aperture radar images using contrast optimization," *IEEE Trans. Aerosp. Electron.Syst.*, vol.32, no. 7, pp. 1185-1191, Jul. 1996.
5. J. R. Fienup and J. J. Miller, "Aberration correction by maximizing generalized sharpness metrics," *J. Opt. Soc. Amer. A*, vol. 20, no. 4, pp. 609-620, Apr. 2003.
6. C. E. Mancill and J. M. Swiger, "A map drift autofocus technique for correcting higher-order SAR phase errors," in *Proc. 27th Annual Tri-Service Radar Symp.*, Monterey, CA, Jun. 1981, pp. 391-400.
7. T.C. Colloway and G. Donohoe, "Subaperture Autofocus for Synthetic Aperture Radar," *IEEE Transactions on Aerospace and Electronic Systems*, Vol. 30, No. 2, pp. 617-621, April 1994.
8. M. Çetin and W. C. Karl, "Feature-enhanced synthetic aperture radar image formation based on non-quadratic regularization," *IEEE Trans. Image Processing* 10, pp. 623-631, Apr. 2001.
9. "Air Force Research Laboratory, Model Based Vision Laboratory, Sensor Data Management System MSTAR Web Page: <http://www.mbvlab.wpafb.af.mil/public/sdms/datasets/mstar/>."
10. "Backhoe Data Sample & Visual-D Challenge Problem available through the Air Force Research Laboratory Sensor Data Management System Web Page: <https://www.sdms.afml.af.mil/main.htm>."
11. Kak A. C. ve Slaney M., "Principles of computerized tomographic imaging," IEEE Press, New York, 1988.
12. M. Çetin and R. L. Moses, "SAR Imaging from Partial-Aperture Data with Frequency-Band Omissions", *Proc. SPIE*, Vol. 5808, 2005.